Assessment of Differential Doppler Navigation with Starlink LEO Satellite Signals of Opportunity

Samer Hayek, Joe Saroufim, Mohammad Neinavaie, Sharbel Kozhaya, and Zaher M. Kassas
The Ohio State University

BIOGRAPHY

Samer Hayek is a Ph.D student in the Department of Electrical and Computer Engineering at The Ohio State University and a member of the Autonomous Systems Perception, Intelligence, and Navigation (ASPIN) Laboratory. He received a B.E. in Mehchanical Engineering from the Lebanese American University. His current research interests include low Earth orbit satellites, autonomous vehicles, sensor fusion, and simultaneous localization and mapping.

Joe Saroufim is a Ph.D student in the Department of Electrical and Computer Engineering at The Ohio State University and a member of the ASPIN Laboratory. He received a B.E. in Mechanical Engineering from the Lebanese American University. His current research interests include low Earth orbit satellites, situational awareness, autonomous vehicles, and sensor fusion.

Mohammad Neinavaie is a Ph.D. student at The Ohio State University and member of the ASPIN Laboratory. He received a B.E. in Electrical Engineering and an M.S. in digital communication systems from Shiraz University. His research interests include opportunistic navigation, cognitive radio, wireless communication systems, and software-defined radio.

Sharbel Kozhaya is a Ph.D student in the Department of Electrical and Computer Engineering at The Ohio State University and a member of the ASPIN Laboratory. He received a B.E. in Electrical Engineering from the Lebanese American University. His current research interests include opportunistic navigation, low Earth orbit (LEO) satellites, software-defined radio, signal fusion, and 5G.

Zaher (Zak) M. Kassas is a Professor at The Ohio State University and director of the ASPIN Laboratory. He is also director of the U.S. Department of Transportation Center: CARMEN (Center for Automated Vehicle Research with Multimodal AssurEd Navigation), focusing on navigation resiliency and security of highly automated transportation systems. He received a B.E. in Electrical Engineering from the Lebanese American University, an M.S. in Electrical and Computer Engineering from The Ohio State University, and an M.S.E. in Aerospace Engineering and a Ph.D. in Electrical and Computer Engineering from The University of Texas at Austin. He is a recipient of the National Science Foundation (NSF) CAREER award, Office of Naval Research (ONR) Young Investigator Program (YIP) award, Air Force Office of Scientific Research (AFOSR) YIP award, IEEE Walter Fried Award, Institute of Navigation (ION) Samuel Burka Award, and ION Col. Thomas Thurlow Award. He is a ION Fellow and an IEEE Aerospace and Electronic Systems Society Distinguished Lecturer. His research interests include cyber-physical systems, navigation systems, autonomous vehicles, and intelligent transportation systems.

ABSTRACT

A framework for differential Doppler navigation with Starlink low Earth orbit (LEO) space vehicle (SV) signals of opportunity is presented, and the framework's performance is assessed. The differential framework assumes a rover (vehicle) navigating without global navigation satellite system (GNSS) signals, through the simultaneous tracking and navigation (STAN) approach. In STAN, the vehicle aids its inertial navigation system (INS) with Doppler measurements extracted from LEO SVs via an extended Kalman filter (EKF), simultaneously estimating the vehicle's and LEO SVs' states. In addition, the differential framework assumes a stationary base with a known position, making Doppler measurements to the same Starlink LEO SVs and communicating these measurements with the rover. The objective of the proposed differential framework is to mitigate the effects of poorly known LEO SVs' ephemerides, unknown LEO SVs' dynamic clock error states, and atmospheric delays. Simulation results are presented to assess the performance of the proposed differential framework compared to a non-differential STAN. The simulations assume an aerial vehicle equipped with a tactical-grade inertial measurement unit (IMU) and an altimeter, navigating for 28 km in 300 seconds, the last 23 km of which without GNSS, while receiving signals from 14 Starlink LEO SVs. It is shown that the non-differential STAN achieves a position root-mean squared error (RMSE) of 15.63 m, while the differential STAN with one, two, and three bases reduces the position RMSE to 5.26 m, 3.88 m, and 1.94 m, respectively. Experimental results are presented in which a stationary base and a stationary rover, located at a distance of 1 km apart, extract Doppler observables from 3 Starlink LEO SVs. The differential framework was able to estimate the rover's three-dimensional (3-D) and 2-D position with an error of 33.4 m and 5.6 m, respectively.

I. INTRODUCTION

The advent of recent and upcoming low Earth orbit (LEO) satellite megaconstellations is shaping a new era of satellite-based navigation. LEO-based communication has been offered over the past couple of decades by LEO constellations; such as Orbcomm, Iridium, and Globalstar; each of which composed of tens of LEO space vehicles (SVs). However, the launch of LEO megaconstellations; such as Starlink, OneWeb, Kuiper, Telesat, SpaceMobile; which are aggregately planning to launch tens of thousands of LEO SVs is promising to revolutionize several domains, bringing unprecedented high-resolution images; remote sensing; and global, high-availability, high-bandwidth, and low-latency Internet [1–3].

Due to LEO satellites' inherently desirable attributes, namely: (i) geometric and spectral diversity, (ii) abundance, (iii) high received signal power, and (iv) high orbital velocity, LEO satellites offer an attractive alternative to global navigation satellite systems (GNSS), which reside in medium Earth orbit (MEO) [4–7]. The promise of utilizing LEO SVs for navigation has been the subject of numerous recent theoretical [8–16] and experimental [17–25] studies. While some of these studies proposed to design LEO satellite constellations dedicated for navigation [26–30] other studies proposed to exploit LEO satellite signals for navigation purposes [31–33]. The latter approach essentially follows the school of thought of exploiting terrestrial signals of opportunity, which has shown tremendous potential in recent years: achieving meter-level accuracy on ground vehicles [34–38], indoors [39–42], and on high-altitude aircraft [43, 44]; submeter-level accuracy on low-altitude aircraft [45–48]; and being usable in environments under intentional GPS jamming [49, 50].

However, several challenges need to be addressed before LEO SV signals could be reliably used for navigation. First, in contrast to GNSS satellites that periodically transmit their positions in the navigation message, LEO SV ephemerides cannot be accurately obtained. The complete ephemeris data of each active satellite is publicly available as two-line-element (TLE) files, published by the North American Aerospace Defense Command (NORAD) [51]. Each TLE file is comprised of six Keplerian elements (inclination, right ascension of ascending node, eccentricity, argument of perigee, mean anomaly, and mean motion) which characterize the LEO SV's position at a specific time epoch. The TLE files can be readily used to initialize orbit propagation algorithms, such as the Simplified General Perturbations (SGP4) [52] model to estimate the positions and velocities of satellites, but the orbit propagation causes position errors on the order of kilometers, and hence, becomes unsuitable for accurate positioning and navigation solutions. Second, unlike GNSS satellites that are equipped with atomic and tightly synchronized clocks, LEO SVs are not necessarily as tightly synchronized nor are equipped with atomic clocks. Third, although LEO SVs are located at relatively low altitudes from the surface of the Earth, their signals propagate through the ionosphere and the troposphere, which induce delays in the received signal, which corrupt the extracted navigation observables.

Previous research addressed the aforementioned challenges by developing the simultaneous tracking and navigation (STAN) framework, originally proposed in [53]. STAN utilizes LEO observables to aid the inertial navigation system (INS) of a navigating vehicle, while simultaneously estimating the position, velocity, and clock states of the orbiting LEO satellites. The framework was demonstrated through simulations as well as experimentation, where a navigation solution was produced using LEO observables when GNSS signals were unavailable [54]. Recent studies that evaluated the performance of STAN suggested that increasing the number of LEO satellites used compensates for lower quality inertial measurement units (IMUs) and that the quality of the receiver's clock has a noticeable effect on the resulting navigation solution [55].

Differential positioning methods entail deducing measurement errors for a certain satellite using a stationary reference antenna with a known position, and communicating these error corrections to connected navigating users [56]. These satellite errors that are compensated for by differential methods include clock calibration, ephemeris errors, and ionospheric and tropospheric delays [57]. A differential carrier-phase navigation system with GPS and LEO SVs was presented in [58]. Moreover, differential navigation with carrier phase measurements from Orbcomm LEO SVs was demonstrated in [59, 60] and with Doppler measurements from Iridium NEXT LEO SVs and Starlink LEO SVs were studied in [61] and [62], respectively.

This paper demonstrates the benefit of differential Doppler measurements from Starlink LEO satellites to improve both: a mobile vehicle navigating via STAN and a stationary receiver localizing itself. The paper presents the following contributions. First, a single difference framework is introduced into the STAN framework to reduce errors due to LEO SVs' ephemerides, clock errors, and ionospheric and tropospheric delays. Second, in order to validate the benefit of adopting the differential Doppler measurement model, a simulation study is conducted to compare two configurations: (i) standalone STAN where the vehicle relies solely on the measurements extracted from its receiver and (ii) differential STAN where the vehicle differences its measurements from those communicated from a reference base station.

The simulation assumed an aerial vehicle equipped with a tactical-grade IMU and an altimeter, navigating for 28 km in 300 seconds, the last 23 km of which without GNSS, while receiving signals from 14 Starlink LEO SVs. It is shown that the non-differential STAN achieves a position root-mean squared error of 15.63 m, while the differential STAN with one, two, and three bases reduces the position RMSE to 5.26 m, 3.88 m, and 1.94 m, respectively. In addition, an experiment is conduced in which a stationary base and a stationary rover, located at a distance of 1 km apart, extract Doppler observables from 3 Starlink LEO SVs. The differential framework was able to estimate the rover's three-dimensional (3-D) and 2-D position with an error of 33.4 m and 5.6 m, respectively.

The rest of the paper is organized as follows. Section II describes the STAN with differential measurements framework. Section III presents the simulation study. Section IV presents experimental results showcasing the potential of differential Doppler measurements on receiver localization. Section V gives concluding remarks.

II. DIFFERENTIAL DOPPLER POSITIONING FRAMEWORK

1. Vehicle Dynamics

The navigating vehicle's state vector $\boldsymbol{x}_r$, shown in Fig. 1, is composed of ${}^{b}_{g}\bar{\boldsymbol{q}}$, which is a four-dimensional quaternion vector representing the orientation of the body frame $\{\mathrm{b}\}$ fixed at the IMU with respect to the global frame $\{\mathrm{g}\}$, $\boldsymbol{r}_r$ and $\dot{\boldsymbol{r}}_r$ are the 3-D position and velocity of the vehicle expressed in $\{\mathrm{g}\}$, and $\boldsymbol{b}_{gyr}$ and $\boldsymbol{b}_{acc}$ denote the 3-D biases of the IMU's gyroscope and accelerometer, respectively, expressed in $\{\mathrm{b}\}$ [53].

2. LEO Satellite Dynamics

The position and velocity of a LEO SV can be estimated using the open-loop SGP4 orbit propagator that is initialized from a TLE file. However, SGP4-generated ephemeris suffer from errors on the order of a few kilometers [63]. Therefore, the proposed framework adopts the STAN paradigm, where the LEO SV position and velocity states are simultaneously estimated in a closed-loop fashion. The two-body J2 model is employed to propagate the LEO SV dynamics as it possesses desirable error characteristics for use in the STAN framework, and has a known analytical expression for the state transition Jacobian [64]. The model is defined by the instantaneous gravitational acceleration of the Earth and resolves the three-dimensional position and velocity vectors of the LEO SV as described in [63, 64]. The state vector of the l-th LEO SV $\boldsymbol{x}_{leo,l}$ shown in Fig. 1, is composed of the satellite's position $\boldsymbol{r}_{leo,l}$ and velocity $\dot{\boldsymbol{r}}_{leo,l}$ vectors.

3. Clock Dynamics

Since LEO SV Doppler measurements are a function of the receiver and satellite clock drifts, the latter has to be estimated as part of the system's state. Although the satellite clock drifts are eliminated in the differential measurement model, the relative clock drifts of the rover and the base cannot be resolved. Hence, this clock state is modeled to evolve according to the clock dynamics used in the carrier-phase differential navigation in [59]. This relative clock difference is estimated as part of the rover's state vector shown in Fig. 1, and is represented by $\delta t^{(R,B)}$ and $\dot{\delta} t^{(R,B)}$, denoting the relative clock bias and drift, respectively.

4. Measurement Model

Previous literature has demonstrated receiver structures that are able to extract Doppler frequency observables from Starlink LEO satellite signals [24, 25]. The Doppler measurement f_D extracted by the LEO receiver is related to the pseudorange rate measurement $\dot{\rho}$ according to

$$\dot{\rho} = -\frac{c}{f_c} f_D, \tag{1}$$

where f_c is the LEO SV carrier frequency. The pseudorange rate measurement from the i-th receiver to the l-th LEO satellite is modeled as

$$\dot{\rho}^{(i)}_{l}(k) = [\dot{\boldsymbol{r}}_{r,i}(k) - \dot{\boldsymbol{r}}_{leo,l}(k)]^{\mathsf{T}} \frac{\boldsymbol{r}_{r,i}(k) - \boldsymbol{r}_{leo,l}(k)}{\|\boldsymbol{r}_{r,i}(k) - \boldsymbol{r}_{leo,l}(k)\|_2} + c \cdot [\dot{\delta} t_{r,i}(k) - \dot{\delta} t_{leo,l}(k)] + c\dot{\delta} t^{(i)}_{trop,l}(k) + c\dot{\delta} t^{(i)}_{iono,l}(k) + \nu^{(i)}_{\dot{\rho},l}(k), \tag{2}$$

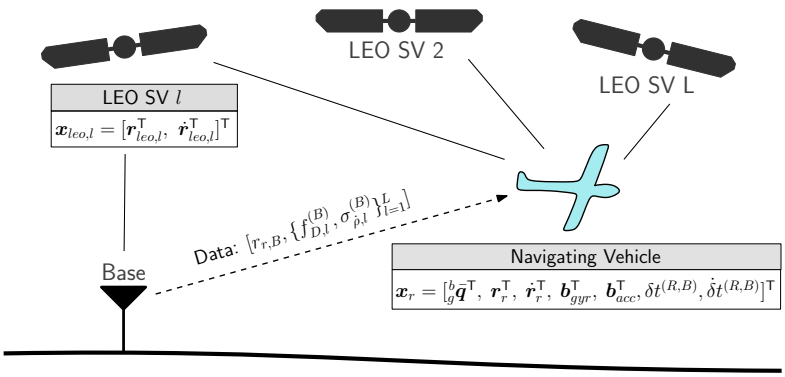

Figure 1: Navigating vehicle and base station in the differential Doppler navigation framework

where $\dot{\boldsymbol{r}}_{r,i}$ and $\dot{\boldsymbol{r}}_{leo,l}$ are the 3-D velocity vectors, of the i-th receiver and the l-th LEO SV in the Earth-Centered Earth-Fixed (ECEF) reference frame, respectively; $\dot{\delta}t_{r,i}$ and $\dot{\delta}t_{leo,l}$ are the clock drifts of the i-th receiver and the l-th LEO SV, respectively; $\dot{\delta}t^{(i)}_{iono,l}$ and $\dot{\delta}t^{(i)}_{trop,l}$ are the ionospheric and tropospheric delay rates (drifts), respectively; and $\nu^{(i)}_{\dot{\rho},l}$ is the pseudorange rate measurement noise, which is modeled as a discrete-time zero-mean white Gaussian sequence with standard deviation $\sigma^{(i)}_{\dot{\rho},l}$. Note that the i-th receiver denotes the base (B) or the rover (R).

The differential pseudorange rate measurement model across the rover and the base is defined as:

$$\begin{aligned} z^{(R,B)}_l(k) &= \dot{\rho}^{(R)}_l(k) - \dot{\rho}^{(B)}_l(k) \\ &= [\dot{\boldsymbol{r}}_{r,R}(k) - \dot{\boldsymbol{r}}_{leo,l}(k)]^{\mathsf{T}} \frac{\boldsymbol{r}_{r,R}(k) - \boldsymbol{r}_{leo,l}(k)}{\|\boldsymbol{r}_{r,R}(k) - \boldsymbol{r}_{leo,l}(k)\|_2} - [\dot{\boldsymbol{r}}_{r,B}(k) - \dot{\boldsymbol{r}}_{leo,l}(k)]^{\mathsf{T}} \frac{\boldsymbol{r}_{r,B}(k) - \boldsymbol{r}_{leo,l}(k)}{\|\boldsymbol{r}_{r,B}(k) - \boldsymbol{r}_{leo,l}(k)\|_2} \\ &\quad + c\dot{\delta}t^{(R,B)}_r(k) + c\dot{\delta}t^{(R,B)}_{trop,l}(k) + c\dot{\delta}t^{(R,B)}_{iono,l}(k) + \nu^{(R,B)}_l(k), \end{aligned} \tag{3}$$

where

$$\begin{aligned} \dot{\delta}t^{(R,B)}_r(k) &\triangleq \dot{\delta}t^{(R)}_r(k) - \dot{\delta}t^{(B)}_r(k) \\ \dot{\delta}t^{(R,B)}_{trop,l}(k) &\triangleq \dot{\delta}t^{(R)}_{trop,l}(k) - \dot{\delta}t^{(B)}_{trop,l}(k) \\ \dot{\delta}t^{(R,B)}_{iono,l}(k) &\triangleq \dot{\delta}t^{(R)}_{iono,l}(k) - \dot{\delta}t^{(B)}_{iono,l}(k) \\ \nu^{(R,B)}_{\dot{\rho},l}(k) &\triangleq \nu^{(R)}_{\dot{\rho},l}(k) - \nu^{(B)}_{\dot{\rho},l}(k). \end{aligned}$$

The difference of Doppler measurements obtained at the base and the rover presents the following advantages to the resulting measurement model: (i) the dynamic clock drifts of the LEO SVs are eliminated as both receivers are processing signals transmitted by the same satellites and (ii) the differences between the ionospheric and tropospheric drifts at the base and the rover are negligible when the receivers are relatively close. Note that for the differenced measurement model, the measurement noise variance is equal to the summation of the measurement noise variances at the base and the rover.

III. SIMULATION RESULTS

This section presents simulation results illustrating the potential of the Differential STAN framework described in Section II.

1. Simulation Setup

The study considered a fixed-wing unmanned aerial vehicle (UAV) traveling a 28 km trajectory in 300 seconds over Columbus, Ohio, USA, and a varying number of base stations. The UAV was equipped with a tactical-grade IMU, an altimeter, and a GNSS receiver. GNSS pseudoranges were fused with altimeter measurements to aid the onboard INS for the first 60 seconds of flight time, before cutting off GNSS signals for the remaining 240 seconds. Furthermore, the UAV was equipped with a Starlink LEO receiver producing Doppler measurements during the entire simulation period. Concurrently, the base station was equipped with a GNSS receiver, yielding knowledge of its position. The base generated Doppler observables from the same Starlink LEO satellites. These Doppler observables along with the measurement noise variances at the base were communicated to the rover using the differential framework discussed above. Before GNSS cutoff, the vehicle operated in Tracking mode: the altitude measurements from the altimeter and GNSS receiver were fused in a loosely coupled fashion, while the Doppler observables extracted by the Starlink receiver were used by the EKF to estimate the LEO satellites's states and rover-base(s) clock error differences as explained in Sections II.2 and II.3, respectively. After GNSS cutoff, the UAV integrates the measurements from the altimeter and Starlink satellites alone, along with the received observables from the base(s), to simultaneously localize the UAV and estimate the LEO satellites' and clock errors' states.

The IMU measurements including the gyroscope and accelerometer readings were generated from the UAV's kinematics according to Section II.1 with the bias instability and noise density parameters for a tactical-grade IMU as documented in Table 1. The UAV and base stations were equipped with a high-quality oven-controlled crystal oscillator (OCXO) clocks, while the LEO SVs were simulated as chip-scale atomic clocks (CSACs). The process noise of each clock was derived from the power-law coefficients listed in Table 1. The LEO satellites' ground truths were generated on Analytical Graphics Inc. (AGI) Systems Tool Kit (STK), which used TLE files of 14 Starlink Satellites taken on January 9, 2023, at 17:00 UTC and propagated using High Precision Orbit Propagator (HPOP) giving the positions and velocities of the satellites during the simulation period. These tracked LEO SVs were visible from Columbus with a minimum elevation of 15 degrees.

Table 1: Simulation Settings

IMU Parameters	
Gyroscope Bias Instability	1.5° / hr
Gyroscope Noise Density	1.5° / hr / $\sqrt{\text{Hz}}$
Accelerometer Bias Instability	100 μg
Accelerometer Noise Density	110 $\mu\text{g}/\sqrt{\text{Hz}}$
Oscillator Power Law Coefficients	
High-quality OCXO $\{h_0, h_{-2}\}$	$\{2.6 \times 10^{-22}, 4.0 \times 10^{-26}\}$
CSAC $\{h_0, h_{-2}\}$	$\{7.2 \times 10^{-21}, 2.7 \times 10^{-27}\}$
Altimeter	
Measurement noise variance	1 m^2

To demonstrate the potential of differential LEO measurements, this paper studied the vehicle's navigation performance using three configurations: (i) standalone INS where the UAV relied solely on the IMU, (ii) stanalone STAN where the UAV navigated using Doppler observables extracted from its LEO receiver alone, and (iii) differential-STAN where measurements from the base(s) were communicated to the UAV and differenced from its own measurements.

2. Results

Fig. 2 shows the EKF error plots for the UAV's position and velocity states for the three configurations (the differential-STAN assumed only 1 base). Note the rapid divergence of the $\pm 3\sigma$ estimation error bounds in the east and north directions corresponding to the GNSS-INS solution after GNSS cutoff, while the STAN position errors appear to diverge at a slower rate. Note that STAN velocity errors in the east and north directions diverge much slower compared to the corresponding position state errors, indicating that the velocity states are more observable. On the other hand, upon introducing a single base into STAN, the error divergence rate reduces dramatically.

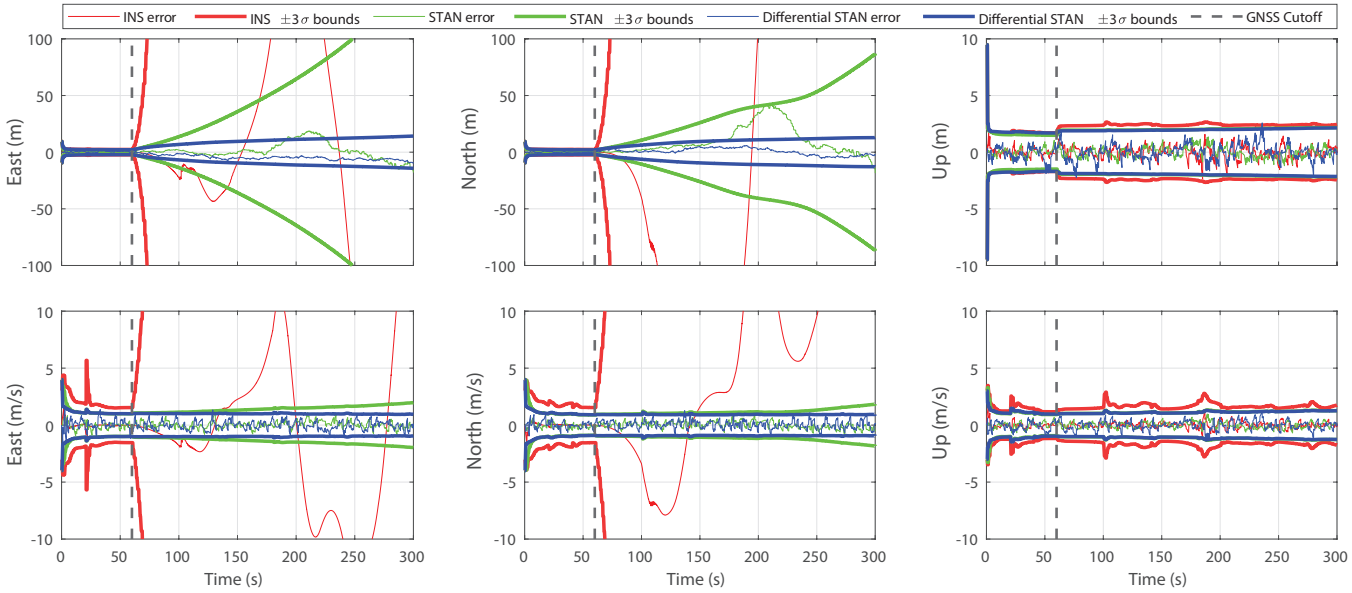

Figure 2: EKF estimation error plots and $\pm 3\sigma$ bounds of the UAV states for: (i) GNSS-INS and (ii) LEO Doppler-aided INS STAN, and (iii) LEO Doppler-aided INS Differential-STAN (single base). The first and second rows correspond to the position and velocity states, respectively, of the vehicle in the East-North-Up (ENU) frame.

Fig. 3 illustrates the effect of varying the number of base stations on the $\pm 3\sigma$ estimation error bounds of the rover's positions in the ENU frame in comparison with the STAN and GNSS-INS configurations. It can be seen that the error bounds shrink dramatically with the addition of the first base, and become slightly tighter with the integration of the second and third bases,

where the maximum deviations in the East and North directions are 10 m and 9.1 m with two bases, then 8.2 m and 7.2 m with three bases, respectively.

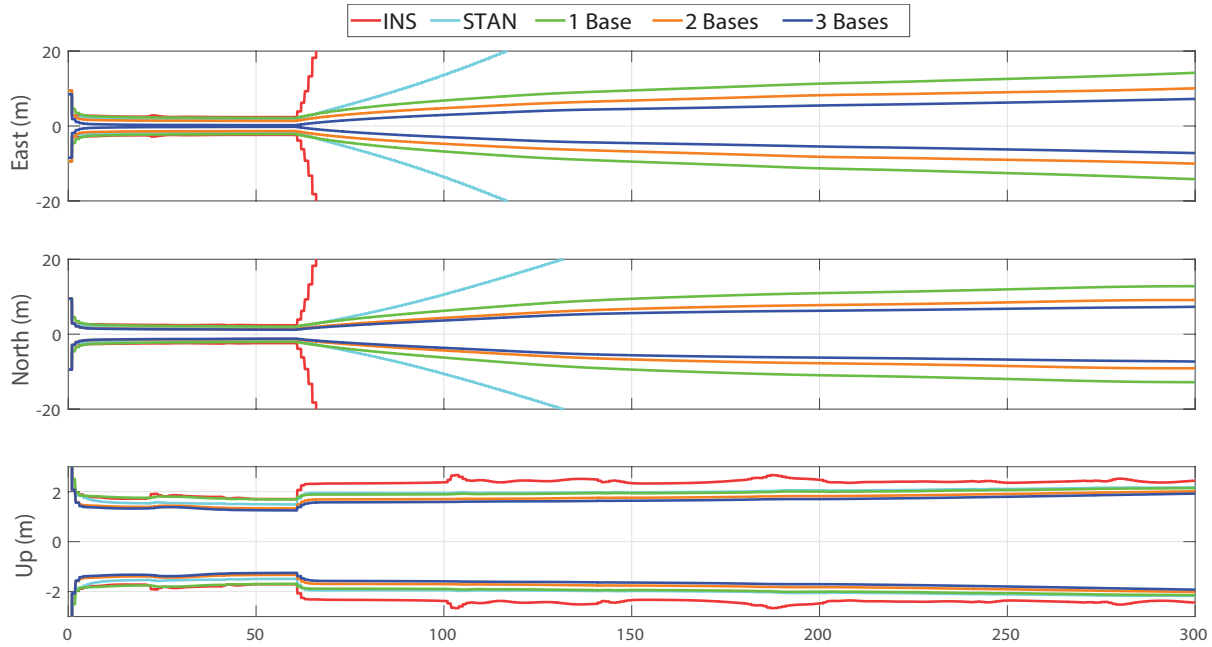

Figure 3: EKF $\pm 3\sigma$ estimation error bounds of the aerial vehicle states in the ENU frame with Doppler-aided INS for varying number of base stations.

The 14 Starlink satellites were tracked during the simulation period via STAN and differential-STAN. Fig. 4 shows the EKF estimation $\pm 3\sigma$ error bounds for Starlink-1154 with STAN, and differential-STAN with varying number of bases. The EKF plots show the reduction in uncertainty of the satellite's estimated positions with the number of bases.

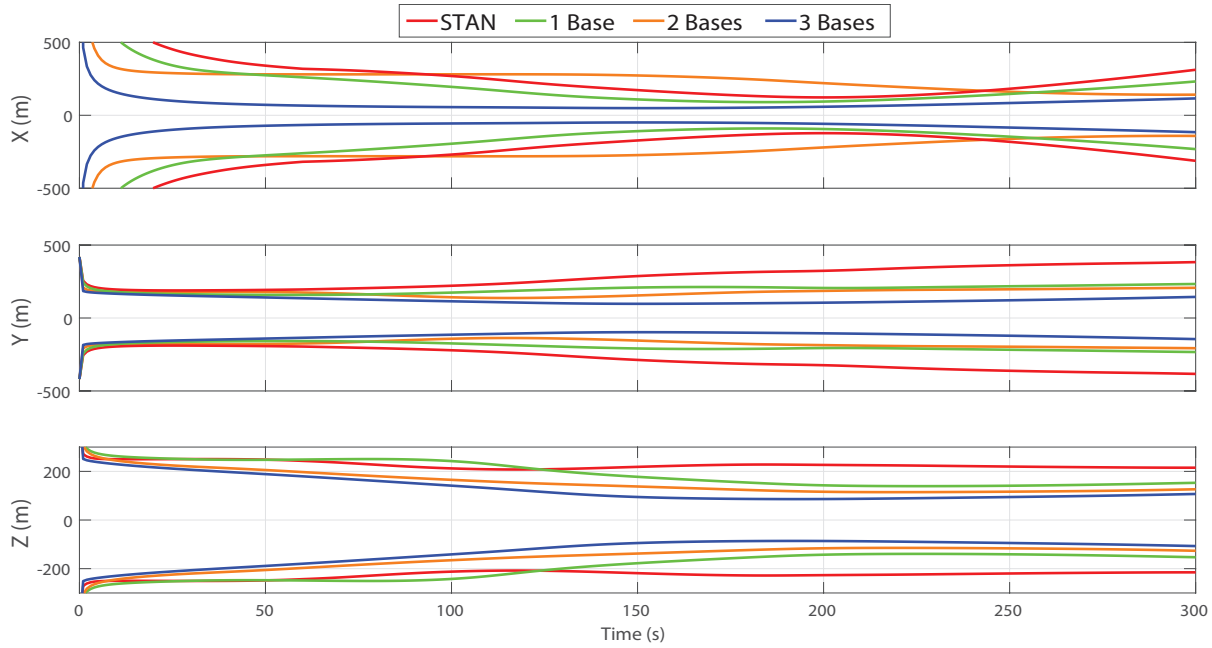

Figure 4: EKF $\pm 3\sigma$ estimation error bounds of the Starlink-1154 LEO SV position states in the ECEF frame tracked for varying number of base stations.

Fig. 5 summarizes shows the UAV's ground truth trajectory along with the navigation results with three configurations. It also shows the locations of the 3 base stations. Table 2 summarizes the UAV's navigation performance.

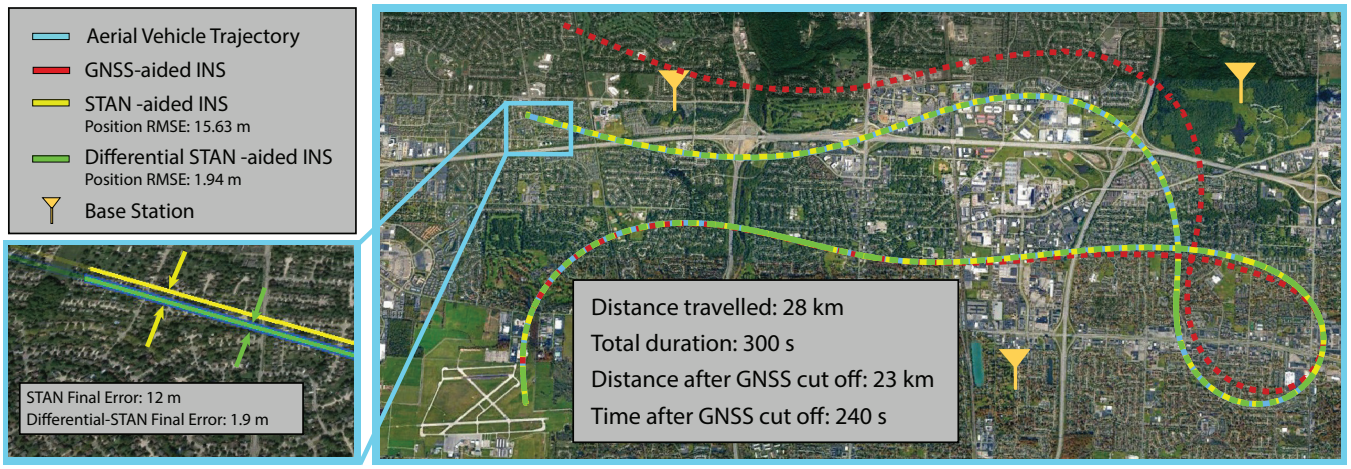

Figure 5: Simulation results showing the aerial vehicle's trajectory and estimated trajectory with GNSS-aided INS, STAN, and Differential STAN with three base stations. Map data: Google Earth.

Table 2: Summary of Simulation Results

	GNSS-INS	**STAN**	**Differential-STAN**		
			1 Base	2 Bases	3 Bases
RMSE (m)	528	15.63	5.26	3.88	1.94
Final Error (m)	1795	25.79	9.54	2.05	1.90

IV. EXPERIMENTAL RESULTS: STATIONARY RECEIVER POSITIONING

This section presents experimental results of receiver positioning with differential Doppler measurements from Starlink LEO SV signals. The experiment was conducted in Irvine, California, USA and consisted of two receivers: a base with a known position and a rover with unknown position, located at a distance of 1.004 km away from each other.

1. Experimental Setup

The hardware setup for the experimental demonstration was described in [62]. The base was equipped with an Ettus E312 universal software defined radio peripheral (USRP), a consumer-grade Ku antenna, and a low-noise block (LNB) downconverter to receiver Starlink signals in the Ku band. The rover was equipped with the NI USRP 2974 and the same downconverter used for the base. In addition, both of the base and rover setups included an NI Octoclock to synchronize the clocks of the USRPs and downconverters. The sampling rate was set to 2.5 MHz, and the carrier frequency was set to 11.325 GHz, which is one of the Starlink downlink frequencies. The received signal samples were stored for off-line post-processing.

2. Differential Doppler Positioning Results

The LEO receivers on-board the base and rover recorded signals from 3 Starlink LEO SVs: Starlink 44740, 48295, and 47728, which were visible for 320 seconds.

A weighted nonlinear least squares (WNLS) algorithm was used to estimate the position of the rover as described in [62]. The rover's position estimate was initialized at a distance of approximately 200 km from the base. The 3-D position error was found to be 33.4 m, while the 2-D position error was found to be 5.6 m. Fig. 6 summarizes the experimental results.

Figure 6: (a) Starlink LEO SV trajectories, (b) rover's initial estimate compared to the base/rover's locations, (c) base and rover locations, and (d) true and estimated rover's positions.

V. CONCLUSION

This paper presented a framework demonstrating the potential of differential navigation and localization using LEO Doppler observables from Starlink LEO SVs. A simulation study was conducted on a flying UAV where Doppler LEO observables were fused from its receiver and from a varying number of base stations in a differential-STAN framework. The study showed a significant improvement in both satellites tracking and vehicle navigation as compared to standalone STAN. The results showed a reduction in the UAV's 2-D position RMSE from 15.26 m using standalone STAN, to 1.9 m upon using 3 base stations. Experimental results were presented showing a base placed 1 km away from a stationary rover, making Doppler measurements to 3 Starlink satellites, yielding a 2-D localization error of 5.6 m.

ACKNOWLEDGEMENTS

This work was supported in part by the Office of Naval Research under Grant N00014-19-1-2511, in part by the National Science Foundation (NSF) under Grant 2240512, and in part by the Air Force Office of Scientific Research (AFOSR) under Grant FA9550-22-1-0476.

REFERENCES

[1] A. Yadav, M. Agarwal, S. Agarwal, and S. Verma, "Internet from space anywhere and anytime - Starlink," in *Proceedings of International Conference on Advancement in Electronics & Communication Engineering*, pp. 1–8, July 2022.

[2] A. Judice, K. Venusamy, and J. Livin, "Multilayer LEO satellite constellation coverage analysis and its current research directions," in *Proceedings of IEEE International Conference on Distributed Computing and Electrical Circuits and Electronics*, pp. 1–5, 2022.

[3] N. Okasha, A. Zekry, and F. Newagy, "Hybrid VLC vehicle to vehicle and LEO satellite communication system for highway road coverage," in *Proceedings of International Conference on Computing, Control and Industrial Engineering*, pp. 571–583, 2022.

[4] T. Reid, T. Walter, P. Enge, D. Lawrence, H. Cobb, G. Gutt, M. O'Conner, and D. Whelan, "Position, navigation, and timing technologies in the 21st century," vol. 2, ch. 43: Navigation from low Earth orbit – Part 1: Concept, Current Capability, and Future Promise, pp. 1359–1379, Wiley-IEEE, 2021.

[5] Z. Kassas, "Position, navigation, and timing technologies in the 21st century," vol. 2, ch. 43: Navigation from low Earth orbit – Part 2: models, implementation, and performance, pp. 1381–1412, Wiley-IEEE, 2021.

[6] F. Prol, R. Ferre, Z. Saleem, P. Välisuo, C. Pinell, E. Lohan, M. Elsanhoury, M. Elmusrati, S. Islam, K. Celikbilek, K. Selvan, J. Yliaho, K. Rutledge, A. Ojala, L. Ferranti, J. Praks, M. Bhuiyan, S. Kaasalainen, and H. Kuusniemi, "Position, navigation, and timing (PNT) through low earth orbit (LEO) satellites: A survey on current status, challenges, and opportunities," *IEEE Access*, vol. 10, pp. 83971–84002, 2022.

[7] N. Jardak and Q. Jault, "The potential of LEO satellite-based opportunistic navigation for high dynamic applications," *Sensors*, vol. 22, no. 7, pp. 2541–2565, 2022.

[8] Q. Wei, X. Chen, and Y. Zhan, "Exploring implicit pilots for precise estimation of LEO satellite downlink Doppler frequency," *IEEE Communications Letters*, vol. 24, no. 10, pp. 2270–2274, 2020.

[9] S. Thompson, S. Martin, and D. Bevly, "Single differenced Doppler positioning with low Earth orbit signals of opportunity and angle of arrival estimation," in *Proceedings of ION International Technical Meeting*, pp. 497–509, 2020.

[10] A. Elgamoudi, H. Benzerrouk, G. Elango, and R. Landry, "Gauss Hermite H∞ filter for UAV tracking using LEO satellites TDOA/FDOA measurement—part I," *IEEE Access*, vol. 8, pp. 201428–201440, 2020.

[11] M. Psiaki, "Navigation using carrier Doppler shift from a LEO constellation: TRANSIT on steroids," *NAVIGATION, Journal of the Institute of Navigation*, vol. 68, pp. 621–641, September 2021.

[12] M. Hartnett, "Performance assessment of navigation using carrier Doppler measurements from multiple LEO constellations," Master's thesis, Air Force Institute of Technology, Ohio, USA, 2022.

[13] R. Cassel, D. Scherer, D. Wilburne, J. Hirschauer, and J. Burke, "Impact of improved oscillator stability on LEO-based satellite navigation," in *Proceedings of ION International Technical Meeting*, pp. 893–905, January 2022.

[14] M. Jiang, H. Qin, C. Zhao, and G. Sun, "LEO Doppler-aided GNSS position estimation," *GPS Solutions*, vol. 26, no. 1, pp. 1–18, 2022.

[15] J. Khalife and Z. Kassas, "Performance-driven design of carrier phase differential navigation frameworks with megaconstellation LEO satellites," *IEEE Transactions on Aerospace and Electronic Systems*, vol. 1–20, 2023. accepted.

[16] R. Sabbagh and Z. Kassas, "Observability analysis of receiver localization via pseudorange measurements from a single LEO satellite," *IEEE Control Systems Letters*, vol. 7, no. 3, pp. 571–576, 2023.

[17] M. Leng, F. Quitin, W. Tay, C. Cheng, S. Razul, and C. See, "Anchor-aided joint localization and synchronization using SOOP: Theory and experiments," *IEEE Transactions on Wireless Communications*, vol. 15, pp. 7670–7685, November 2016.

[18] Z. Tan, H. Qin, L. Cong, and C. Zhao, "New method for positioning using IRIDIUM satellite signals of opportunity," *IEEE Access*, vol. 7, pp. 83412–83423, 2019.

[19] F. Farhangian and R. Landry, "Multi-constellation software-defined receiver for Doppler positioning with LEO satellites," *Sensors*, vol. 20, pp. 5866–5883, October 2020.

[20] F. Farhangian, H. Benzerrouk, and R. Landry, "Opportunistic in-flight INS alignment using LEO satellites and a rotatory IMU platform," *Aerospace*, vol. 8, no. 10, pp. 280–281, 2021.

[21] K. Wang and A. El-Mowafy, "LEO satellite clock analysis and prediction for positioning applications," *Geo-spatial Information Science*, vol. 25, no. 1, pp. 14–33, 2022.

[22] C. Huang, H. Qin, C. Zhao, and H. Liang, "Phase - time method: Accurate Doppler measurement for Iridium NEXT signals," *IEEE Transactions on Aerospace and Electronic Systems*, vol. 58, no. 6, pp. 5954–5962, 2022.

[23] M. Li, T. Xu, M. Guan, F. Gao, and N. Jiang, "LEO-constellation-augmented multi-GNSS real-time PPP for rapid re-convergence in harsh environments," *GPS Solutions*, vol. 26, no. 1, pp. 1–12, 2022.

[24] J. Khalife, M. Neinavaie, and Z. Kassas, "The first carrier phase tracking and positioning results with Starlink LEO satellite signals," *IEEE Transactions on Aerospace and Electronic Systems*, vol. 56, pp. 1487–1491, April 2022.

[25] M. Neinavaie, J. Khalife, and Z. Kassas, "Acquisition, Doppler tracking, and positioning with Starlink LEO satellites: First results," *IEEE Transactions on Aerospace and Electronic Systems*, vol. 58, pp. 2606–2610, June 2022.

[26] T. Reid, B. Chan, A. Goel, K. Gunning, B. Manning, J. Martin, A. Neish, A. Perkins, and P. Tarantino, "Satellite navigation for the age of autonomy," in *Proceedings of IEEE/ION Position, Location and Navigation Symposium*, pp. 342–352, 2020.

[27] K. Wang and A. El-Mowafy, "Proposed orbital products for positioning using mega-constellation LEO satellites," *Remote Sensing*, vol. 20, pp. 5806–5826, October 2020.

[28] A. Nardin, F. Dovis, and J. Fraire, "Empowering the tracking performance of LEO-based positioning by means of meta-signals," *IEEE Journal of Radio Frequency Identification*, vol. 5, no. 3, pp. 244–253, 2021.

[29] P. Iannucci and T. Humphreys, "Fused low-Earth-orbit GNSS," *IEEE Transactions on Aerospace and Electronics Systems*, 2022. accepted.

[30] D. Egea-Roca, J. Lopez-Salcedo, G. Seco-Granados, and E. Falletti, "Performance analysis of a multi-slope chirp spread spectrum signal for PNT in a LEO constellation," in *Proceedings of Workshop on Satellite Navigation Technology*, pp. 1–9, September 2022.

[31] Z. Tan, H. Qin, L. Cong, and C. Zhao, "Positioning using IRIDIUM satellite signals of opportunity in weak signal environment," *Electronics*, vol. 9, no. 1, p. 37, 2019.

[32] C. Zhao, H. Qin, and Z. Li, "Doppler measurements from multiconstellations in opportunistic navigation," *IEEE Transactions on Instrumentation and Measurement*, vol. 71, pp. 1–9, 2022.

[33] M. Neinavaie, J. Khalife, and Z. Kassas, "Blind Doppler tracking and beacon detection for opportunistic navigation with LEO satellite signals," in *Proceedings of IEEE Aerospace Conference*, pp. 1–8, 2021.

[34] J. Peral-Rosado, J. Lopez-Salcedo, S. Kim, and G. Seco-Granados, "Feasibility study of 5G-based localization for assisted driving," in *Proceedings of International Conference on Localization and GNSS*, pp. 1–6, June 2016.

[35] J. del Peral-Rosado, O. Renaudin, C. Gentner, R. Raulefs, E. Dominguez-Tijero, A. Fernandez-Cabezas, F. Blazquez-Luengo, G. Cueto-Felgueroso, A. Chassaigne, D. Bartlett, F. Grec, L. Ries, R. Prieto-Cerdeira, J. Lopez-Salcedo, and G. Seco-Granados, "Physical-layer abstraction for hybrid GNSS and 5G positioning evaluations," in *Proceedings of IEEE Vehicular Technology Conference*, pp. 1–6, September 2019.

[36] M. Maaref and Z. Kassas, "Autonomous integrity monitoring for vehicular navigation with cellular signals of opportunity and an IMU," *IEEE Transactions on Intelligent Transportation Systems*, vol. 23, pp. 5586–5601, June 2022.

[37] R. Whiton, J. Chen, T. Johansson, and F. Tufvesson, "Urban navigation with LTE using a large antenna array and machine learning," in *Proceedings of IEEE Vehicular Technology Conference*, pp. 1–5, 2022.

[38] C. Yang, M. Arizabaleta-Diez, P. Weitkemper, and T. Pany, "An experimental analysis of cyclic and reference signals of 4G LTE for TOA estimation and positioning in mobile fading environments," *IEEE Aerospace and Electronic Systems Magazine*, vol. 37, no. 9, pp. 16–41, 2022.

[39] M. Ulmschneider and C. Gentner, "Multipath assisted positioning for pedestrians using LTE signals," in *Proceedings of IEEE/ION Position, Location, and Navigation Symposium*, pp. 386–392, April 2016.

[40] A. Abdallah and Z. Kassas, "Multipath mitigation via synthetic aperture beamforming for indoor and deep urban navigation," *IEEE Transactions on Vehicular Technology*, vol. 70, pp. 8838–8853, September 2021.

[41] M. Pan, P. Liu, S. Liu, W. Qi, Y. Huang, X. You, X. Jia, and X. Li, "Efficient joint DOA and TOA estimation for indoor positioning with 5G picocell base stations," *IEEE Transactions on Instrumentation and Measurement*, vol. 71, pp. 1–19, 2022.

[42] L. Chen, X. Zhou, F. Chen, L. Yang, and R. Chen, "Carrier phase ranging for indoor positioning with 5G NR signals," *IEEE Internet of Things Journal*, vol. 9, pp. 10908–10919, July 2022.

[43] Z. Kassas, J. Khalife, A. Abdallah, C. Lee, J. Jurado, S. Wachtel, J. Duede, Z. Hoeffner, T. Hulsey, R. Quirarte, and R. Tay, "Assessment of cellular signals of opportunity for high-altitude aircraft navigation," *IEEE Aerospace and Electronic Systems Magazine*, vol. 37, pp. 4–19, October 2022.

[44] Z. Kassas, J. Khalife, A. Abdallah, C. Lee, J. Jurado, J. Duede, Z. Hoeffner, T. Hulsey, R. Quirarte, S. Wachtel, and R. Tay, "Flight demonstration of high altitude aircraft navigation with cellular signals," *IEEE Intelligent Transportation Systems Magazine*. accepted.

[45] J. Mortier, G. Pages, and J. Vila-Valls, "Robust TOA-based UAS navigation under model mismatch in GNSS-denied harsh environments," *Remote Sensing*, vol. 12, pp. 2928–2947, September 2020.

[46] J. Del Peral-Rosado, P. Nolle, S. Razavi, G. Lindmark, D. Shrestha, F. Gunnarsson, F. Kaltenberger, N. Sirola, O. Särkkä, J. Roström, K. Vaarala, P. Miettinen, G. Pojani, L. Canzian, H. Babaroglu, E. Rastorgueva-Foi, J. Talvitie, and D. Flachs, "Design considerations of dedicated and aerial 5G networks for enhanced positioning services," in *Proceedings of Workshop on Satellite Navigation Technology*, pp. 1–12, April 2022.

[47] J. Khalife and Z. Kassas, "On the achievability of submeter-accurate UAV navigation with cellular signals exploiting loose network synchronization," *IEEE Transactions on Aerospace and Electronic Systems*, vol. 58, no. 5, pp. 4261–4278, 2022.

[48] J. Khalife and Z. Kassas, "Differential framework for submeter-accurate vehicular navigation with cellular signals," *IEEE Transactions on Intelligent Vehicles*, 2022. accepted, doi: 10.1109/TIV.2022.3187957.

[49] Z. Kassas, J. Khalife, A. Abdallah, and C. Lee, "I am not afraid of the GPS jammer: resilient navigation via signals of opportunity in GPS-denied environments," *IEEE Aerospace and Electronic Systems Magazine*, vol. 37, pp. 4–19, July 2022.

[50] A. Abdallah, Z. Kassas, and C. Lee, "Demo: I am not afraid of the GPS jammer: exploiting cellular signals for accurate ground vehicle navigation in a GPS-denied environment," in *Proceedings of Workshop on Automotive and Autonomous Vehicle Security*, pp. 1–1, 2022.

[51] F. Hoots and R. Roehrich, "Spacetrack Report NO. 3." `http://celestrak.com/NORAD/documentation/spacetrk.pdf`, December 1988. Compiled by TS Kelso.

[52] D. Vallado and P. Crawford, "SGP4 orbit determination," in *Proceedings of AIAA/AAS Astrodynamics Specialist Conference and Exhibit*, pp. 6770–6799, August 2008.

[53] Z. Kassas, J. Morales, and J. Khalife, "New-age satellite-based navigation – STAN: simultaneous tracking and navigation with LEO satellite signals," *Inside GNSS Magazine*, vol. 14, no. 4, pp. 56–65, 2019.

[54] Z. Kassas, M. Neinavaie, J. Khalife, N. Khairallah, J. Haidar-Ahmad, S. Kozhaya, and Z. Shadram, "Enter LEO on the GNSS stage: Navigation with Starlink satellites," *Inside GNSS Magazine*, vol. 16, no. 6, pp. 42–51, 2021.

[55] T. Mortlock and Z. Kassas, "Performance analysis of simultaneous tracking and navigation with LEO satellites," in *Proceedings of ION GNSS Conference*, pp. 2416–2429, September 2020.

[56] B. Parkinson and P. Enge, "Differential GPS," *Global Positioning System: Theory and applications.*, vol. 2, pp. 3–50, 1996.

[57] J. Rife, "Collaborative vision-integrated pseudorange error removal: Team-estimated differential GNSS corrections with no stationary reference receiver," *IEEE Transactions on Intelligent Transportation Systems*, vol. 13, no. 1, pp. 15–24, 2011.

[58] M. Rabinowitz, *A Differential Carrier-Phase Navigation System Combining GPS with Low Earth Orbit Satellites for Rapid Resolution of Integer Cycle Ambiguities*. PhD thesis, Stanford University, USA, 2000.

[59] J. Khalife, M. Neinavaie, and Z. Kassas, "Navigation with differential carrier phase measurements from megaconstellation LEO satellites," in *Proceedings of IEEE/ION Position, Location, and Navigation Symposium*, pp. 1393–1404, April 2020.

[60] S. Kozhaya and Z. Kassas, "Blind receiver for LEO beacon estimation with application to UAV carrier phase differential navigation," in *Proceedings of ION GNSS Conference*, 2022. accepted.

[61] C. Zhao, H. Qin, N. Wu, and D. Wang, "Analysis of baseline impact on differential doppler positioning and performance improvement method for LEO opportunistic navigation," *IEEE Transactions on Instrumentation and Measurement*, pp. 1–10, 2023.

[62] M. Neinavaie, Z. Shadram, S. Kozhaya, and Z. M. Kassas, "First results of differential Doppler positioning with unknown Starlink satellite signals," in *Proceedings of IEEE Aerospace Conference*, pp. 1–14, March 2022.

[63] N. Khairallah and Z. Kassas, "Ephemeris closed-loop tracking of LEO satellites with pseudorange and Doppler measurements," in *Proceedings of ION GNSS Conference*, pp. 2544–2555, September 2021.

[64] J. Morales, J. Khalife, U. Santa Cruz, and Z. Kassas, "Orbit modeling for simultaneous tracking and navigation using LEO satellite signals," in *Proceedings of ION GNSS Conference*, pp. 2090–2099, September 2019.